Nano Energy (2014) 8, 238–246

Available online at www.sciencedirect.com

ScienceDirect

journal homepage: www.elsevier.com/locate/nanoenergy

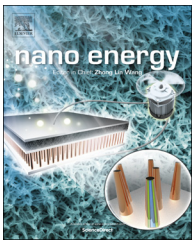

RAPID COMMUNICATION

High performance multi-scaled nanostructured spectrally selective coating for concentrating solar power

Jaeyun Moon[a,c,1], Dylan Lu[b,1], Bryan VanSaders[b,c], Tae Kyoung Kim[a,c], Seong Deok Kong[a,c,2], Sungho Jin[a,c], Renkun Chen[a,c,*], Zhaowei Liu[b,c,*]

[a]Department of Mechanical Engineering, University of California, San Diego, La Jolla, CA 92093, USA
[b]Department of Electrical and Computer Engineering, University of California, San Diego, La Jolla, CA 92093, USA
[c]Materials Science and Engineering Program, University of California, San Diego, La Jolla, CA 92093, USA

Received 4 April 2014; received in revised form 23 May 2014; accepted 10 June 2014
Available online 20 June 2014

KEYWORDS
Concentrating solar power;
Effective medium theory;
Multi-scaled nanostructures;
Spectrally selective coating

Abstract
Spectrally selective coatings (SSCs) are a critical component that enables high-temperature and high-efficiency operation of concentrating solar power (CSP) systems. In this Letter, we describe a novel design for a high-performance SSC based on multi-scaled nanostructures. Optimal design of the new structure for high optical performance of the SSC is predicted by the effective medium theory. To demonstrate the feasibility of the design, we fabricate the SSCs using fractal nanostructures with characteristic sizes ranging from ~10 nm to ~10 μm. Optical measurements on these structures show unprecedentedly high performance with ~90–95% solar absorptivity and <30% infrared emissivity near the peak of 500 °C black body radiation. The newly developed concept of SSC could be utilized to design solar absorbers with high thermal efficiency for future high temperature CSP systems.
Published by Elsevier Ltd.

Introduction

Solar energy can potentially play a significant role in the global energy supply [1]. There are two main methods for generating electricity from sunlight: direct solar-electricity conversion using photovoltaic (PV) solar cells and concentrating solar power (CSP) which generates electricity from solar thermal

*Corresponding authors.
E-mail addresses: rkchen@ucsd.edu (R. Chen), zhaowei@ucsd.edu (Z. Liu).
[1]These authors contributed equally to this work.
[2]Current address: Department of Chemical Engineering, University of Texas, Austin, TX 78712, USA.

http://dx.doi.org/10.1016/j.nanoen.2014.06.016
2211-2855/Published by Elsevier Ltd.

energy [2,3]. Despite PV technology's rapid development, CSP still offers several unique advantages: higher energy-conversion efficiency, higher thermal energy storage capability (specifically, a higher capacity factor [4]), and the potential to retrofit current coal power plants. Therefore, large-scale deployment of CSP could enable a higher overall penetration of solar energy [5]. As of 2011, the cumulatively installed CSP capacity reached ~1.17 GW, and ~17 GW of CSP is under development worldwide [6].

Among the various components in a CSP system, the solar absorber plays a critical role in overall system performance. To increase the Carnot efficiency of the power generation system, it is desirable that the temperature of the heat transfer fluid (HTF) is 600 °C or higher [7]. In order to increase the temperature of the receiver, a solar absorber has to maximally absorb solar energy while minimizing losses due to black body emission. At a receiver temperature of 500-800 °C, black body emission peaks at wavelengths longer than 2 μm. Most energy within the solar spectrum is located at wavelengths below 2 μm, allowing for the possibility of optimizing receiver performance through tuning the spectral absorptivity (equivalent, at equilibrium, to spectral emissivity). As most materials do not naturally have the desired behavior, engineered composites are needed. Figure 1a illustrates the schematic diagram of a solar absorber with a SSC. An ideal SSC has to exhibit high spectral absorptivity, α_s, in the solar spectrum (0.3-2.0 μm wavelengths), and low spectral emissivity, ε_{IR}, in the IR spectrum (2.0-15 μm wavelengths) (Figure 1b).

The optical performance of the SSC is usually characterized by the ratio of solar absorptivity and IR emissivity at a given operation temperature, which directly dictates the photo-thermal conversion efficiency of solar receivers [8],

$$\eta_{th} = 1 - \frac{Q_{loss}}{Q_{in}} = \alpha_{s,eff} - \frac{\varepsilon_{IR,eff}\sigma(T_R^4 - T_0^4)}{CI} \quad (1)$$

where the effective IR emissivity, $\varepsilon_{IR,eff}$, is defined as,

$$\varepsilon_{IR,eff} = \frac{\int_0^\infty \varepsilon(\lambda)[I_\lambda(T_R,\lambda) - I_\lambda(T_0,\lambda)]d\lambda}{\int_0^\infty [I_\lambda(T_R,\lambda) - I_\lambda(T_0,\lambda)]d\lambda}. \quad (2)$$

and the effective solar absorptivity, $\alpha_{s,eff}$, is determined by,

$$\alpha_{s,eff} = \frac{\int_0^\infty \alpha(\lambda) I_s(\lambda) d\lambda}{\int_0^\infty I_s(\lambda) d\lambda} \quad (3)$$

In the equations, Q_{in} is heat input from the concentrated solar flux, and Q_{loss} is heat loss due to radiation, conduction, and convection heat transfer (negligible when the receiver is placed in an evacuated enclosure). The Stefan-Boltzmann constant is σ ($=5.67 \times 10^{-8}\,\mathrm{Wm^{-2}K^{-4}}$), C stands for the solar concentration ratio and I is the solar insolation. $I_S(\lambda)$ and I_λ (T, λ) are the spectral intensities of solar insolation and blackbody radiation at T, respectively. T_R and T_0 correspond to the temperature of the receiver and ambient, respectively. The spectral absorptivity and emissivity of the SSC are denoted by $\alpha(\lambda)$ and $\varepsilon(\lambda)$, respectively. When the temperature of the HTF is 600 °C or higher for high Carnot efficiency [7], the surface temperature of the SSC would be 700 °C or higher. It is therefore important for SSCs to possess high $\alpha_{s,eff}$ and low $\varepsilon_{IR,eff}$ to satisfy both high operation temperature and power conversion efficiency.

There has been an extensive search for mid- to high-temperature SSC materials [9]. Typical SSC structures fall into one or several of the following schemes: 1. Intrinsic selective materials, the simplest structure usually in the form of thin films with proper intrinsic material selectivity [10]. 2. Semiconductor-metal tandems, which are made from semiconductors with proper bandgaps (E_g~0.5 eV-1.26 eV) that absorb solar radiation in tandem with an underlying metal that provides high IR reflectance. The main drawbacks of this structure include the need for an anti-reflection coating, oxidation of the semiconductors at elevated temperatures, and non-scalable processes for producing semiconductor thin films such as CVD [11] or vacuum sputtering. 3. Multilayer absorbers, which use multilayer stacks of metals and dielectrics to achieve high selectivity due to the interference effect. This scheme is limited by the high cost of the multi-stack fabrication process, such as sputtering and CVD [12,13], as well as high-temperature instability [14]. 4.Textured surfaces, which consist of porous and nano-scale structures for the required spectral selectivity through optical trapping of sunlight [15]. The spectral emittance can be adjusted by modifying the microstructure of the coating. However, these highly textured metal surfaces tend to degrade quickly at elevated temperature [16,17]. 5. Metal-dielectric composites, which utilize a highly solar-absorbent and IR-transparent material deposited onto a highly IR-reflective

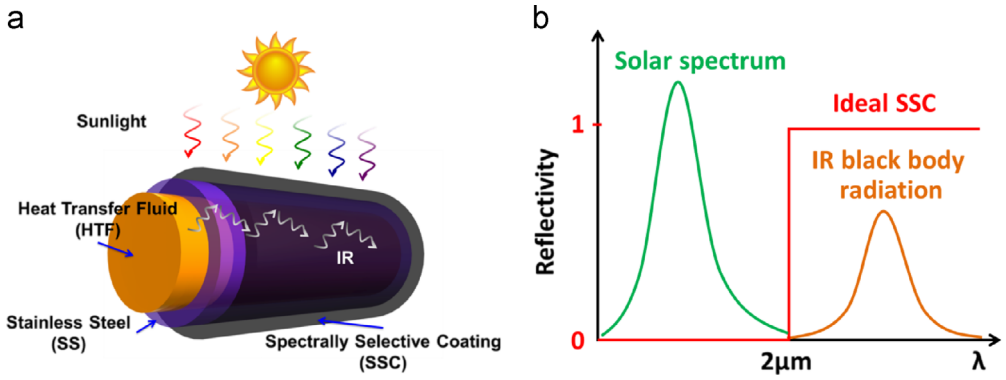

Figure 1 Spectrally selective coating (SSC) for concentrated solar power. (a) Schematic of a solar absorber with stainless steel (SS) tube coated with the SSC. (b) Optical reflectance of an ideal SSC. In the solar spectrum (short wavelength), the reflectance is zero (or the absorptance is 100%); in the IR spectrum, the reflectance is 100% (or the emittance is zero). Such an ideal SSC will have the maximum absorptance for solar energy but with minimal heat loss due to the blackbody IR thermal radiation of the absorber itself.

metal substrate. The 'black' absorbing layer is a cermet of fine metal particles in a dielectric matrix [18-20]. This design offers a very high degree of flexibility for tuning the absorption and scattering cutoff wavelengths by particle and matrix constituents, particle sizes and concentrations, coating thickness, etc.

Based on the above discussion, it is evident that an ideal and practical SSC material and scheme has yet to be identified [9,21]. Current SSCs typically have a high solar absorptivity but they either need high cost and vacuum processes, such as CVD and sputtering, or do not have a good spectral selectivity at around 1-2 μm. In addition, most SSC materials degrade after prolonged operation at high temperatures, which is unsatisfactory for future CSP operation at high temperature ($\geq 700\ ^{\circ}C$). In this Letter, we demonstrated a high-performance SSC based on a novel design of multi-scaled semiconductor particles with sizes ranging from ~ 10 nm to ~ 10 μm. The micro/nano multi-scale structures, made from a low-cost and scalable coating process, were shown to yield high optical performance by both theoretical modeling and optical measurements.

Theory and calculations

Modeling of multi-scaled SSCs

The design of the multi-scaled SSC described in this Letter combines several features offered by the existing SSCs summarized above. As shown in Figure 2, our approach is based on semiconductor nanoparticles deposited on highly IR-reflective metal surfaces, which utilizes the concepts of the 'intrinsic semiconductor', 'textured surface' and 'metal-dielectric composite' approaches. First, we employed a semiconductor material with a suitable band gap for the selectivity at around 1-2 μm wavelength, which is similar to the 'intrinsic semiconductor' scheme. Secondly, we utilized multi-scale structures with a wide range of particle sizes in order to induce an appropriate surface morphology leading to higher light absorption. Since the multi-scaled nanostructures increase light trapping efficiency ('textured surfaces' scheme), there is no need for an additional anti-reflection coating layer. This is parallel to an extremely efficient anti-reflection coating in PV solar cells by using nanostructures to reduce the impedance mismatch and enhance light trapping [22]. However, our multi-scaled structures can be readily achieved by a simple coating process, which is more cost effective than previously reported methods [22] using lithography and etching processes in crystalline Si. Lastly, the composite structure of semiconductor powders and dielectric matrix reported here was inspired by the 'metal-dielectric composite' concept that is flexible and versatile.

As a guideline for the fabrications of the SSC structures, we simulate optical properties of a SSC material that is comprised of nanoparticles embedded in a dielectric host with its representative cross-sectional view shown in Figure 2a. An effective-medium-theory-based model was applied by approximating the nanostructured SSC to a two-layer geometry as shown in Figure 2b. The effective medium approximation treats the uniform nano-composite metamaterial (nanoparticles in the dielectric host) as an isotropic medium with a thickness of L_1 and an effective permittivity determined by the permittivities of individual components, i.e. ε_p for nanoparticles and ε_h for the dielectric host [23-25], and respective volumetric ratios. The surface-structured metamaterial with a thickness of L_2 can thus be treated as a gradient-refractive-index (GRIN) layer mixed between the uniform metamaterials and air. The GRIN layer is modeled by discretizing the material into infinitesimally thin layers in the vertical direction, each of which may be considered as a uniform medium. Determined by the particle filling ratio of the coating, the effective dielectric function for both uniform and GRIN layers follows the Maxwell-Garnett formalism or the Bruggeman mixing theory [24]. The GRIN layer gradually smoothes out the permittivity discontinuity between air and the uniform metamaterial layer, thus serving as a perfect anti-reflection layer.

The reflectance of the total structure can be calculated using a transfer matrix method once the effective permittivities are known [26]. Figure 3a shows numerically simulated reflectance spectra of the SSC with different nanoparticle filling ratios at normal incidence based on the Bruggeman mixing theory [27]. In the simulation, the uniform metamaterial layer is assumed to be made of intrinsic Si nanoparticles embedded in a SiO_2 host, with the corresponding permittivities taken from Refs. [28,29]. The GRIN layer is divided into 100 individual uniform layers with effective permittivities varying smoothly from air to that of the

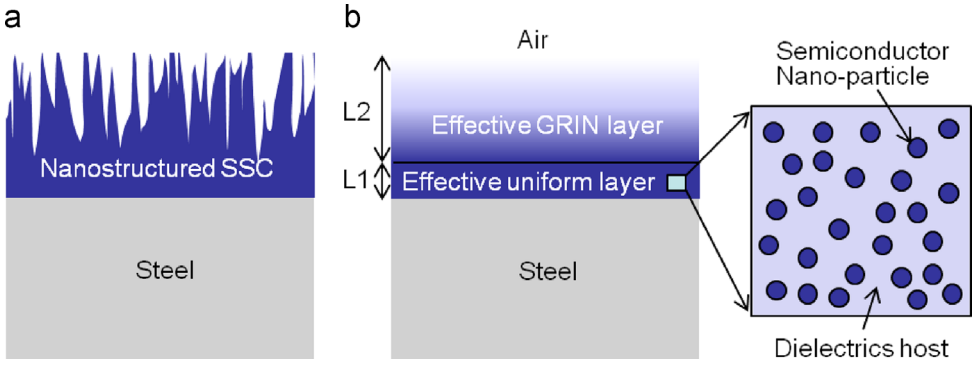

Figure 2 Optical modeling system for the SSC. The nanostructured SSC in (a) is modeled by a multilayer system consisting of a gradient refractive index layer with a thickness of L_2 and a uniform effective layer with a thickness of L_1 on the SS substrate as schematically shown in (b). The effective layer corresponds to the semiconductor nanoparticles in the dielectric host. The effective material properties can be described by the effective medium theory when the particle size is much smaller than the operation wavelengths.

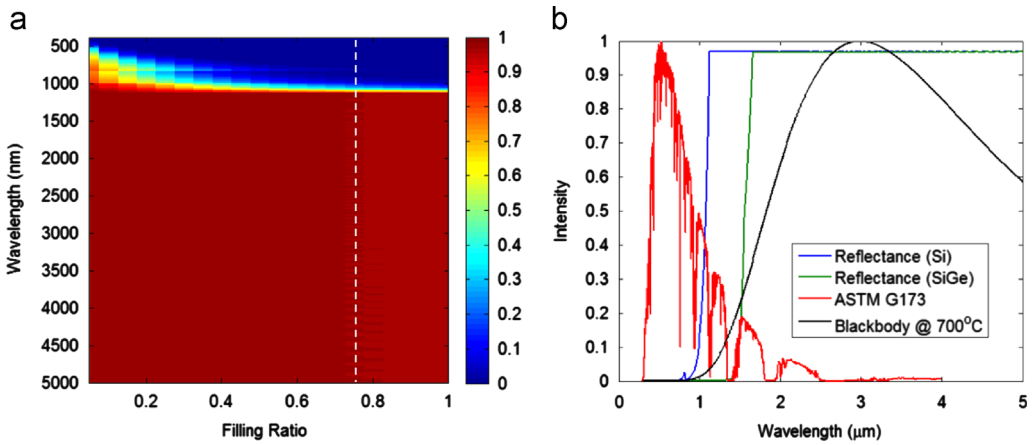

Figure 3 Numerical simulation results of the reflectance spectra for the SSC. (a) Reflectance with respect to incident wavelengths and the volumetric filling ratios of the nanoparticles where the incident angle is fixed at 0° (normal incidence). The materials of the nanoparticles and dielectric host are Si and SiO_2, respectively. L_1=20 μm, L_2=10 μm. (b) Reflectance of the SSC layer when the filling ratio of the nanoparticles is equal to 0.75 (blue line), i.e., at the location marked by the dashed vertical line in (a). Reflectance of the SSC layer (green) made of SiGe (volumetric filling ratio of Si in SiGe, 80%) in SiO_2 host with the same nanoparticle filling ratio, normalized standard solar spectrum in red and the blackbody radiation at 700 °C in black are also added for comparison.

bulk layer. When the particle filling ratio exceeds 50%, a sharp change is observed in the reflectance spectra of the simulated coating near wavelengths of 1.1 μm, corresponding to the bandgap of Si. Figure 3b shows a reflectance curve (blue line) when the Si filling ratio is 75% as compared with the standard solar spectrum and the blackbody radiation spectrum at 700 °C. The comparison indicates that the solar absorptivity, α, for the SSC device is close to 99% while its IR emissivity, ε, is about 4%. It is worth noting that the optical properties of the SSC layer with different semiconductor and dielectric combinations are always similar, except that the cutoff wavelengths may shift according to the bandgap of the semiconductor. The reflectance curve (green line) for the SiGe with a same filling ratio of 75% in an SiO_2 host indicates that the cutoff wavelength shifts to a longer wavelength with composition change.

From the calculations, it is clear that the following factors are the primary causes of the overall high performance. Firstly, the effective GRIN layer acts as a perfect light trapping or anti-reflection layer. In practice, the Bruggeman mixing theory used here will be a valid approximation when features of the layer are sub-wavelength to incident radiation (<300 nm for visible light). Secondly, an appropriate nanoparticle material and its volumetric filling ratio are the key parameters for tuning the cutoff wavelength in the reflectance spectra. Lastly, a smooth steel layer underneath improves reflectance at IR wavelengths. The surface roughness of steel should be deep sub-wavelength at IR frequencies (typically <100 nm) to reduce the IR absorption due to surface light trapping. Although not shown here, the calculated reflectance is almost invariant to light polarizations and incident angles, indicating the robustness of the SSC layer.

Materials and methods

Fabrication of multi-scaled SSCs

To validate the new design, we used $Si_{0.8}Ge_{0.2}$ as a representative semiconductor material to fabricate SSCs. $Si_{0.8}Ge_{0.2}$ is expected to yield the desirable light absorptivity in VIS-NIR range (<1 μm) due to the intrinsic bandgap of $Si_{0.8}Ge_{0.2}$, ~1.04 eV [30]. The $Si_{0.8}Ge_{0.2}$ powders of various sizes were prepared by a spark erosion process. Spark erosion is a process originally developed by Berkowitz and Walter [31] for rapid production of semiconductor and metallic powders. We recently modified the process for high-yield production of nano-sized powders [32]. Figure 4a is a schematic diagram of the spark erosion process. Two electrodes of $Si_{0.8}Ge_{0.2}$ are mounted in a cell and connected to a pulsed power source. During the spark erosion process, a high temperature spark (micro-plasma) is produced and vaporizes the materials of charges (small pieces) and electrodes in the localized region. When the spark collapses, vaporized material and molten droplets are ejected into the dielectric liquid (liquid Ar in this case), where they are rapidly quenched to produce clean nanoparticles with different sizes. In order to induce sparks, the charges and electrodes should be electrically conductive. Therefore, $Si_{0.8}Ge_{0.2}$ materials used for a spark erosion process were slightly doped by phosphorus (P). Following spark erosion, attrition milling was carried out with the spark eroded $Si_{0.8}Ge_{0.2}$ particles for optimizing the particle size distribution to increase the proportion of powders of several hundred nanometers, which are strong scatterers of the range of incident light wavelengths.

Figure 4b and c shows SEM and TEM pictures of the spark-eroded $Si_{0.8}Ge_{0.2}$ particles. These images show that the particles have a wide range of powder sizes, ranging from ~10 nm to 10 μm due to the high quenching rate presented in the spark erosion process. This is a distinct difference from many other particle synthesis techniques [33,34], which usually yield mono-dispersed particle sizes. As we shall show later, the multi-scaled particles are very beneficial to SSC applications compared to the uniform ones.

A simple coating process was employed to deposit the particles onto a polished stainless steel (SS) surface. As shown in Figure 4d, the as-made $Si_{0.8}Ge_{0.2}$ particles were dispersed into an organic solvent, and the solution was

Figure 4 SSC sample preparation. (a) Schematic diagram of the spark erosion process. (b) SEM, (c) TEM of the spark-eroded $Si_{0.8}Ge_{0.2}$powders. (d) Schematic of the coating process for making SSC samples: 1, dispersion of nanoparticles in solvent; 2, sonication; 3, drop casting of the solution on a SS substrate; 4, drying and annealing.

sonicated to make a uniform mixture. Concentration of the solutions was controlled and kept consistent. The nanoparticle solution was then coated onto targeted substrates by drop casting. After the solvent dried, a coating film made of $Si_{0.8}Ge_{0.2}$ particles was formed on the SS substrate. The film thickness was controlled to ~100 μm by adjusting the drop casting conditions. In order to demonstrate the effect of particle-size distribution, ~100-μm-thick films made from commercial Si powders (Alfa Aesar) with average diameter of ~100 nm were also prepared using the same process.

We also performed brief high temperature tests for the SiGe coating at 750 °C for 1 h in air environment. The particular condition was chosen because 750 °C is higher than the current operation temperature of the high temperature CSP (550 °C) but lower than the melting point of $Si_{0.8}Ge_{0.2}$ (~1270 °C). Even though this material can be used in a vacuum enclosure, the oxidation resistance is also desired in case the vacuum was unintentionally breached. Further systematic high temperature durability tests as well as oxidation protective coating need to be performed to evaluate the applicability of the new SSC for future CSP systems.

Results and discussion

The fabricated SSC samples were characterized by SEM. Figure 5a and b shows top-view SEM images of the SSC layer made by using spark-eroded Si–Ge particles. After deposition, micro-scale dome-shaped structures are built up by micro-sized spark-eroded particles. These micro-scale particles are covered with nano-scale powders as shown in Figure 5b, thus creating the multi-scale features. In order to study the effect of multi-scaled structure on light absorption, we also prepared mono-dispersed powder sample which was made using Si nanoparticles with uniform size of ~100 nm, as shown in Figure 5c and d. Unlike spark-eroded Si–Ge particles, the top surface of the Si coating is

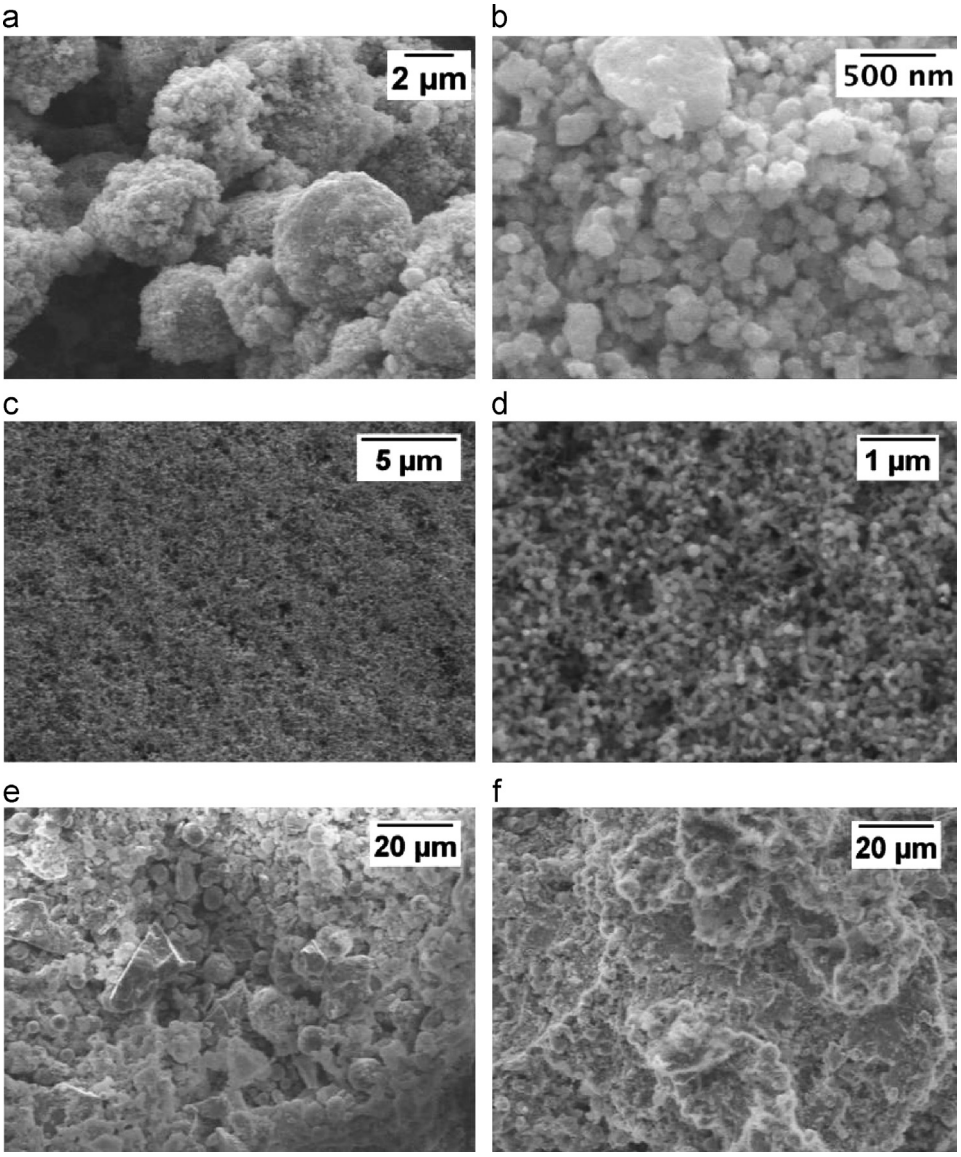

Figure 5 Characterization of the SSCs. (a and b), SEM images of the SSC based on spark-eroded $Si_{0.8}Ge_{0.2}$ particles. (c and d), SEM images of the SSC made by ~100 nm Si nanoparticles. SEM images of the same Si-Ge sample (e) before and (f) after annealing at 750 °C in air for 1 h.

quite smooth except for the roughness at the particle size scale. Figure 5e and f shows the SEM images of the same SSC before and after annealing at 750 °C for 1 h in air, respectively. It is evident that the morphology of the SSC remains similar after the annealing test.

The optical reflectance of the SSCs was measured by a UV-visible spectrometer and directional emission at a temperature of 500 °C measured in a Fourier transform infrared (FTIR) spectrometer, with the results presented in Figure 6a and b, respectively. To characterize the SSCs in the UV-visible range, incident light from Xenon lamp was focused onto the sample surface which was contained within an integration sphere capable of collecting all angles of scattered light. Collected spectra were analyzed by an ANDOR™ Shamrock 303i spectrograph equipped with a Newton 920 CCD detector. High temperature IR emittance was characterized by an FTIR spectrometer (Mattson Galaxy5020) with custom built heated sample stage. The samples were kept under vacuum during measurement to reduce heat loss, and a maximum temperature of samples reached 500 °C. A sample of Pyromark 2500 (Tempil) was used as a standard reference for the measurement, with directional emissivity data taken from Ref. [35]. As shown in Figure 6a, the multi-scaled SSC layers made from the spark-eroded powders have low reflectivity of 5-10% across the UV-NIR solar spectrum. In contrast, the SSC made from uniform Si nanoparticles shows much higher reflectivity (13-80%). This demonstrates the high light-trapping efficiency of the multi-scaled structures: if the particles are all micro-sized, light will be reflected from the surface of large particles; on the other hand, if the particles are all nano-sized, the uniform surface of the SSC layer will result in inefficient light trapping, as in the case of the control sample made by 100-nm Si nanoparticles. Similar multi-scaled structure has been achieved using lithographic patterning for enhanced light absorption in PV devices

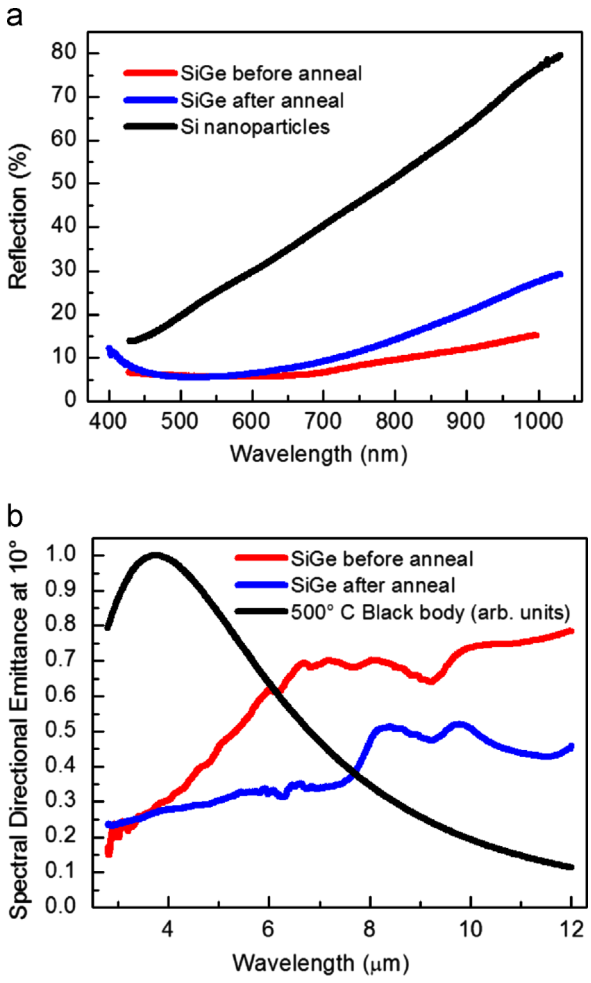

Figure 6 (a) Measured reflectance of the SSCs in the UV to near-IR regime. (b) Measured IR emission spectra at 500 °C. The black curve in (b) is the normalized blackbody spectrum at 500 °C.

[22,36,37]. In addition to the light trapping effect, the lower bandgap of Si-Ge particles enables more absorption than Si particles in the spectrum range below bandgap of Si-Ge (~1.2 μm). And in the aspect of mass production, the approach we developed is based on multi-scaled particles naturally formed during the spark-erosion process and the following attrition milling, and hence is more readily applicable for large-scale applications such as CSP. Further optimization of the coating, including material selection, particle size distribution, and coating morphology, is likely to reduce the solar reflectivity further, as shown in our simulation results (Figure 3a). The optimal parameters such as the particle size range and distribution warrant further investigation.

Figure 6b shows the directional spectral emittance of SiGe SSC layers at IR frequencies. Rough surfaces generally display isotropic (Lambertian) scattering and we can therefore expect the presented data to be representative of all-angle emission spectra. The SiGe sample shows low emission below 0.3 near the peak of 500 °C black body radiation which stems from the low absorption coefficient obtained by the light with energy below the bandgap of $Si_{0.8}Ge_{0.2}$, (~1.04 eV or 1.2 μm). The discrepancy between simulated (Figure 3b) and experimental emission spectra at IR is mainly attributed to the excitation of considerable hot carriers at elevated temperature.

We also evaluated the potential of the multiscale structural SSCs for high temperature operation ($\geq$700 °C). The blue curves in Figure 6a and b shows the reflectance of the Si-Ge SSC sample after annealing at 750 °C for 1 h in air. Even though $Si_{0.8}Ge_{0.2}$ can be oxidized at high temperature in air environment, we observed the annealed sample exhibited a small increase in the reflectance in the UV-VIS-NIR range. This coincides with the structural observation showing minimal morphological and structural changes of the particles after the annealing [Figure 5(e-g)]. In order to improve high temperature stability, a comprehensive study and oxidation degradation needs to be conducted in future researches. Furthermore, the application of high temperature durable materials having appropriate band gaps, such as conductive oxides, will be a promising approach.

Conclusions

We reported the design and fabrication of a new SSC structure based on multi-scaled semiconductor nanostructures. The Si-Ge SSC is highly absorbent for short-wavelength photons (with energy higher than the semiconductor bandgap) and efficiently reflective for long-wavelength photons. The measured spectral solar reflectance (5-10%) and IR emissivity (<30%) of the SSC indicate high performance for CSP applications. We also found that the multi-scale features (10 nm-10 μm) of the particles have significantly enhanced the solar absorptivity compared to uniform nanoparticles due to the more efficient light trapping. The particles and the SSC are made by spark erosion and low-cost drop casting process, which is applicable for making large-scale solar absorbers. We anticipate the high solar absorptance and low IR emittance of the developed SSC will significantly benefit future high temperature CSP technologies by improving their maximum attainable temperature and thermal efficiency. In addition, the SSC shows the potential to maintain the multi-scale structure and optical properties after high temperature process. Further applications of the multi-scaled structure on high temperature materials and systematic high temperature durability tests will be performed to evaluate the applicability of the new SSC for future high temperature CSP systems.

Acknowledgments

This work is supported by U.S. Department of Energy, SunShot Program Contract no. DE-EE005802 and The University of California Proof of Concept Award ID# 12-PC-246854. We are grateful for Prof. A. Berkowitz for the use of the spark-erosion system and P. Nguyen for assistance on spark erosion.

References

[1] N.S. Lewis, Science 315 (2007) 798-801.
[2] H. Price, E. Lupfert, D. Kearney, E. Zarza, G. Cohen, R. Gee, R. Mahoney, J. Sol. Energy-T ASME 124 (2002) 109-125.
[3] V. Quaschning, Sol. Energy 77 (2004) 171-178.
[4] I. Gur, K. Sawyer, R. Prasher, Science 335 (2012) 1454-1455.

[5] P. Denholm, M. Mehos, National Renewable Energy Laboratory, 2011.
[6] U. Wang, The Rise of Concentrating Solar Thermal Power. Renewable Energy World.com. Available from: ⟨http://www.renewableenergyworld.com/rea/news/article/2011/06/the-rise-of-concentrating-solar-thermal-power⟩, June 6, 2011.
[7] S. Chu, A. Majumdar, Nature 488 (2012) 294–303.
[8] J.A. Duffie, W.A. Beckman, Book Solar Engineering of Thermal Processes, Wiley, New York, 1991.
[9] C.E. Kennedy, NREL Technical Report, National Renewable Energy Laboratory, 2002.
[10] Z.C. Orel, B. Orel, M.K. Gunde, Sol. Energy Mater. Sol. C 26 (1992) 105–116.
[11] A. Donnadieu, B.O. Seraphin, J. Opt. Soc. Am. 68 (1978) 292–297.
[12] D.D. Allred, M.R. Jacobson, E.E. Chain, Sol. Energy Mater. 12 (1985) 87–129.
[13] B.O. Seraphin, Thin Solid Films 57 (1979) 293–297.
[14] J.A. Thornton, J.L. Lamb, Thin Solid Films 96 (1982) 175–183.
[15] L.K. Thomas, E.E. Chain, Thin Solid Films 105 (1983) 203–211.
[16] M. Lira-Cantu, A.M. Sabio, A. Brustenga, P. Gomez-Romero, Sol. Energy Mater. Sol. C 87 (2005) 685–694.
[17] S.N. Patel, O.T. Inal, A.J. Singh, A. Scherer, Sol. Energy Mater. 11 (1985) 381–399.
[18] A. Andersson, O. Hunderi, C.G. Granqvist, J. Appl. Phys. 51 (1980) 754–764.
[19] V. Teixeira, E. Sousa, M.F. Costa, C. Nunes, L. Rosa, M.J. Carvalho, M. Collares-Pereira, E. Roman, J. Gago, Thin Solid Films 392 (2001) 320–326.
[20] C.E. Kennedy, H. Price, in: Proceedings of International Solar Energy Conference, Orlando, Florida USA, 2005.
[21] E. Randich, D.D. Allred, Thin Solid Films 83 (1981) 393–398.
[22] F. Toor, M.R. Page, H.M. Branz, H.-C. Yuan, in: Proceedings of the 37th IEEE Photovoltaic Specialists Conference, Seattle, Washington, 2011.
[23] W. Cai, D.A. Genov, V.M. Shalaev, Phys. Rev. B 72 (2005) 193101.
[24] J. Sancho-Parramon, V. Janicki, H. Zorc, Opt. Express 18 (2010) 26915.
[25] D. Lu, J. Kan, E.E. Fullerton, Z. Liu, Appl. Phys. Lett. 98 (2011) 243114.
[26] P. Yeh, Book Optical Waves in Layered Media, Wiley, Hoboken, NJ, 2005.
[27] Similar Reflectance Spectra are Also obtained Based on the Maxwell–Garnett Formalism. Since the Work Focuses on Large Filling Ratios, Only Results Based on the Bruggeman Mixing Theory is Shown Since it Provides More Appropriate Effective-medium Description for Large Nanoparticle Filling Ratios.
[28] D.E. Aspnes, A.A. Studna, Phys. Rev. B 27 (1983) 985.
[29] M.J. Weber, Book Handbook of Optical Materials, CRC Press, Boca Raton, 2003.
[30] R. Braunstein, A.R. Moore, F. Herman, Phys. Rev. 109 (1958) 695–710.
[31] A.E. Berkowitz, J.L. Walter, J. Mater. Res. 2 (1987) 12.
[32] P.-K. Nguyen, K.H. Lee, J. Moon, S.I. Kim, K. Ahn, L.-H. Chen, S.M. Lee, R. Chen, S. Jin, A. Berkowitz, Nanotechnology 23 (2012) 415604.
[33] D. Gerion, N. Zaitseva, C. Saw, M.F. Casula, S. Fakra, T. Van Buuren, G. Galli, Nano Lett. 4 (2004) 597–602.
[34] G. Joshi, H. Lee, Y.C. Lan, X.W. Wang, G.H. Zhu, D.Z. Wang, R.W. Gould, D.C. Cuff, M.Y. Tang, M.S. Dresselhaus, G. Chen, Z.F. Ren, Nano Lett. 8 (2008) 4670–4674.
[35] C.K. Ho, A.R. Mahoney, A. Ambrosini, M. Bencomo, A. Hall, T.N. Lambert, J. Sol. Energy Eng. 136 (2014).
[36] A.R. Parker, Z. Hegedus, R.A. Watts, P Roy Soc Lond B Bio 265 (1998) 811–815.
[37] A.R. Parker, H.E. Townley, Nat. Nanotechnol. 2 (2007) 347–353.

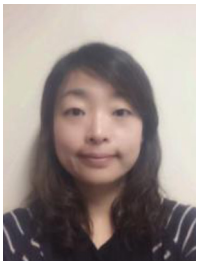

Jaeyun Moon is a Ph.D. candidate in the Materials Science and Engineering Program at the University of California, San Diego (UCSD). She obtained her B.S. and M.S. degree from Hanyang University (South Korea) and had worked at Samsung Electronics as a senior engineer and then joined UCSD in 2009 as a research assistant. She has focused on renewable energy generation, especially thermal energy conversion, such as concentrated solar power and thermoelectrics.

Dylan Lu is a Ph.D. candidate in the Department of Electrical and Computer Engineering at the University of California, San Diego (UCSD). He obtained his B.S. and M.S. degree from Nanjing University (China) and Hong Kong University of Science and Technology, respectively, before joining UCSD in 2009 as a research assistant. He has focused on nanostructured materials including metamaterials for advanced plasmonic and energy applications.

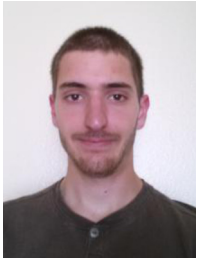

Bryan VanSaders is a Ph.D. graduate student in the Material Science and Engineering department at the University of California San Diego (UCSD). He obtained his B.S. degree from Rutgers University and M.S. degree from UCSD. He has focused on nano-scale optics, plasmonics, and optical metamaterials.

Tae Kyoung Kim is a Ph.D. candidate in the Materials Science and Engineering Program at the University of California, San Diego. He obtained B.S. and M.S. degree from Yonsei University (South Korea) and had worked at Samsung Cheil Inc. as a senior researcher mainly in the field of materials for renewable energy generation and storage systems. And then he has been studying and researching in University of California, San Diego since 2011.

Seong Deok Kong received his Ph.D. in Materials Science & Engineering from UC San Diego in 2010. He is currently a post-doctoral researcher at Chemical Engineering of University of Texas at Austin. His research mainly focuses on synthesis of nano-structured material and its applications on energy and nanomedicine.

Sungho Jin received his B.S degree in Metallurgical Engineering from Seoul National University in 1969, and Ph.D. degree in Materials Science & Engineering from UC Berkeley in 1974. After 26 years of R&D at Bell Laboratories at Murray Hill, New Jersey, he joined UC San Diego (UCSD) in 2002 as a Professor and Iwama Endowed Chair. He is currently a Distinguished Professor at UC San Diego, and is serving as the Director of UCSD-wide Materials Science & Engineering Program. His research interests include R&D of nano materials, magnetic materials, electronic materials, energy materials, and bio materials.

Renkun Chen received his B.S. degree in Thermo-physics from Tsinghua University in 2004, and a Ph.D. degree in Mechanical Engineering from the University of California, Berkeley in 2008. Following a one-year stint as a postdoctoral fellow at Lawrence Berkeley National Laboratory, he joined UC San Diego as an Assistant Professor in the Department of Mechanical and Aerospace Engineering in 2009. His research interests include nanoscale heat transfer, energy conversion materials, and thermal management.

Zhaowei Liu is an Assistant Professor of Electrical and Computer Engineering at UCSD. He received his Ph.D. in mechanical engineering (MEMS/Nanotechnology) from UCLA in 2006. Before joining the UCSD faculty, he was a post-doctoral researcher at the NSF Nanoscale Science & Engineering Center (NSEC) in the Mechanical Engineering Department at UC Berkeley. His research interest include nanophotonics, plasmonics, metamaterials, energy and ultrafast optoelectronics.